SCIENCE CHINA
Chemistry

•ARTICLES•

October 2025 Vol.68 No.10: 5039–5050
https://doi.org/10.1007/s11426-025-2666-y

Enantioconvergent deoxygenative reductive cross-coupling of lactic acid derivatives

Li-Li Zhang[1†], Yu-Zhong Gao[2†], Ning Wang[1], Hui Yu[1], Shou-Jie Shen[2], Kaining Duanmu[1*] & Ze-Peng Yang[1*]

[1]*Shanghai Key Laboratory of Chemical Assessment and Sustainability, School of Chemical Science and Engineering, Tongji University, Shanghai 200092, China*
[2]*Key Laboratory of Magnetic Molecules, Magnetic Information Materials, Ministry of Education, School of Chemical and Material Science, Shanxi Normal University, Taiyuan 030031, China*

Received February 11, 2025; accepted March 29, 2025; published online June 26, 2025

As the prominence of green chemistry continues to grow, there is an increasing need to explore and develop alternative energy and fuel sources. Renewable biomass is expected to play a pivotal role in this transition, with lactic acid being particularly noteworthy due to its abundance and affordability. Given its prevalence, lactic acid offers a notable opportunity for transformation into high-value-added products. Here, we describe a method for the enantioconvergent substitution of the hydroxy group at the α-position in lactic acid derivatives by a carbon group, thereby streamlining the synthesis of various bioactive compounds. This reaction achieves both C–O bond cleavage and stereochemical C–C bond formation in a one-pot process. Our approach involves a catalyst system based on nickel and relies on two distinct ligands—a chiral bis(imidazoline) and a phthalimide. Investigations into the underlying mechanisms have provided valuable insights into the role of phthalimide in this process.

lactic acid, photochemistry, deoxygenative, cross-coupling, phthalimide

Citation: Zhang LL, Gao YZ, Wang N, Yu H, Shen SJ, Duanmu K, Yang ZP. Enantioconvergent deoxygenative reductive cross-coupling of lactic acid derivatives. *Sci China Chem*, 2025, 68: 5039–5050, https://doi.org/10.1007/s11426-025-2666-y

1 Introduction

Lactic acid was discovered in 1780 in sour milk, which was then obtained by fermentation in 1881, leading to its large-scale industrial manufacture [1]. By 2022, the global production of lactic acid has exceeded 1 million tons per year [2]. As a prominent form of biomass material, lactic acid occupies a crucial position in a diverse range of biological applications and serves as a vital industrial raw material [3,4]. Being both an alcohol and an acid, lactic acid can undergo intermolecular esterification to yield lactoyllactic acid or lactide; further condensation of lactoyllactic acid can result in the formation of polylactic acid (Figure 1a, top left). Additionally, lactic acid is a cost-effective feedstock for producing several necessary chemicals, including lower alcohol lactates, propylene glycol, and acrylic acid (Figure 1a, top right). From the perspective of an organic chemist, breaking the C–O bond at the α-position in lactic acid and subsequently introducing new functional groups (for example, carbon group) can potentially streamline the synthesis of complex molecules (Figure 1a, bottom). However, such reactions are still rare [5–7]; to our knowledge, an enantioconvergent deoxygenative C-functionalization reaction of lactic acid or its derivatives has not yet been described, despite the fact that enantiopure α-aryl carbonyls are prevalent subunits in numerous pharmaceuticals and bioactive compounds (Figure 1b).

†Equally contributed to this work.
*Corresponding authors (email: duanmukn@tongji.edu.cn; zpyang@tongji.edu.cn)

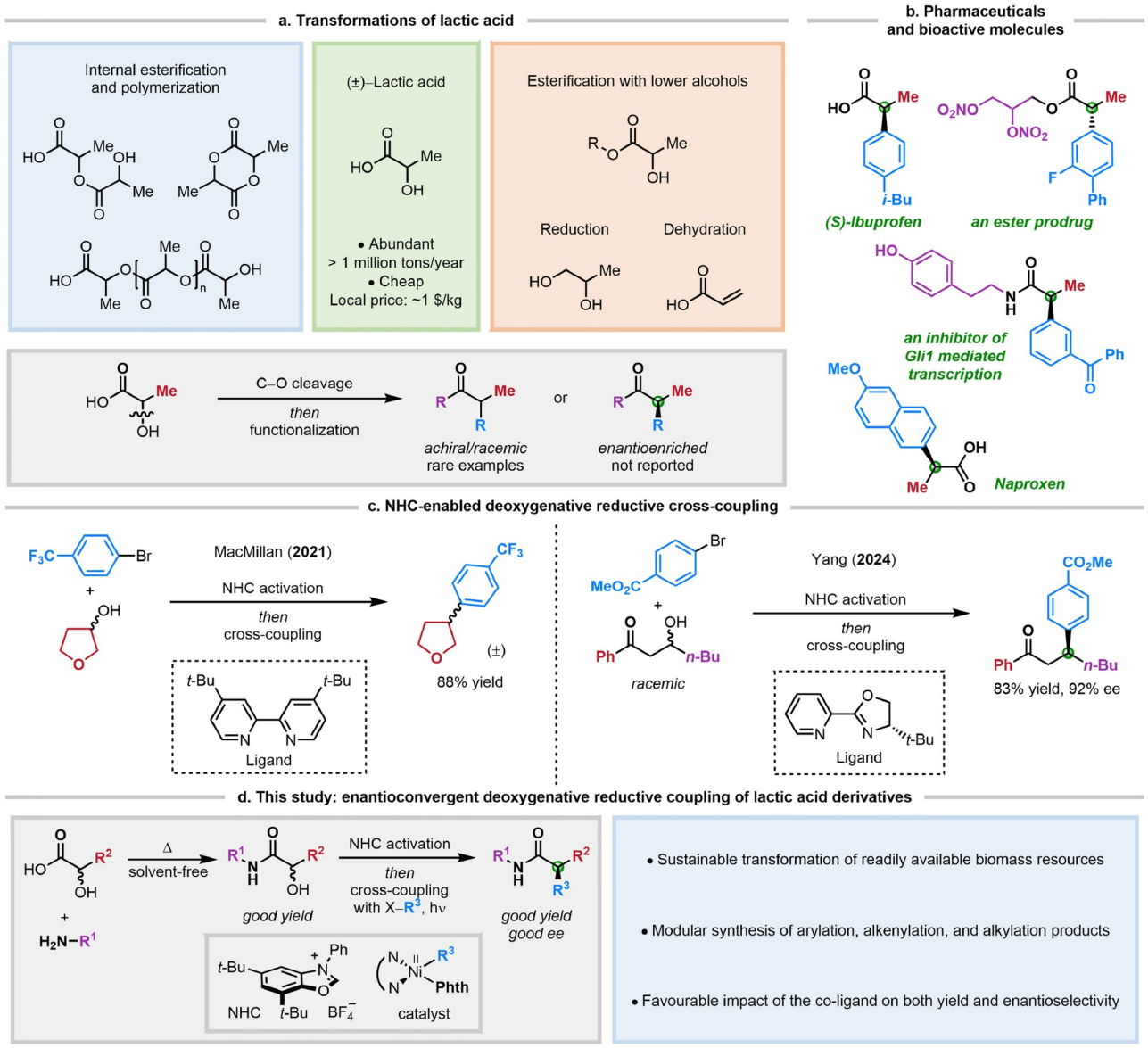

Figure 1 (Color online) Background of this study. (a) Different methods for the transformation of lactic acid. (b) Examples of pharmaceuticals and bioactive molecules. (c) Racemic/achiral and asymmetric NHC-enabled deoxygenative reductive cross-coupling reactions. (d) This study: enantioconvergent deoxygenative reductive cross-coupling of lactic acid derivatives.

In recent years, considerable attention has been given to developing efficient and highly selective methods for forming C–C bonds by utilizing alkyl alcohols as intrinsic sp^3 synthons through C–O cleavage to generate alkyl radical intermediates [8–13]. A key challenge in this area is the high bond dissociation energy of the C–O bond and the limited leaving ability of the OH^- group [14]. Generally, two main strategies have been employed to address this challenge. The first is the direct activation approach used in certain cases, typically with tertiary alkyl alcohols or benzylic alcohols capable of generating relatively stable alkyl radical species [15–26]. In this process, an activating agent is used to directly cleave the C–O bond. The second is the pre-functionalization approach, wherein the robust C–O bond is initially transformed into a weaker C–X bond, followed by the activation of the C–X bond in a subsequent step [27–36]. Ideally, combining pre-functionalization with subsequent activation and transformation into a one-pot process would be optimal [37–43]. In this context, MacMillan's group [44–66] unveiled an elegant NHC (N-heterocyclic carbene) mediated deoxygenative arylation strategy in 2021 (Figure 1c, left). In addition to preserving high efficiency in deoxygenative coupling reactions, managing the stereoselectivity of free radical reactions represents another substantial challenge [67–85]. To this end, our group has demonstrated an enantioconvergent deoxygenative reductive

cross-coupling of β-hydroxy ketone recently (Figure 1c, right) [86–89].

In our pursuit of developing enantioconvergent cross-coupling reactions from readily accessible materials, we envisioned that lactic acid or its derivatives could serve as viable substrates for generating high-value-added compounds through an enantioconvergent deoxygenative coupling process. In this article, we present a comprehensive study on using this strategy for the asymmetric synthesis of α-aryl amides via the coupling of lactic acid derivatives using a dual nickel/photoredox system (Figure 1d). Key to this method is the employment of two ligands: a chiral bis(imidazoline) and a phthalimide, which together afford a chiral nickel catalyst capable of both C–C bond formation and stereochemical control.

2 Experimental

General procedure for enantioconvergent deoxygenative reductive cross-coupling of α-hydroxy amide and aryl bromide: in a nitrogen-filled glovebox, an oven-dried 4 mL vial that contained a stir bar was charged with $NiBr_2$·DME (15.5 mg, 0.051 mmol, 10.0 mol%), (*S*)-**L1** (34.0 mg, 0.060 mmol, 12.0 mol%), and $Ir[dF(CF_3)ppy]_2(dtbbpy)PF_6$ (9.0 mg, 0.0075 mmol, 1.5 mol%). Anhydrous (trifluoromethyl)benzene (2.5 mL) was added, and the vial was capped with a PTFE septum cap. The mixture was stirred at room temperature for 30 min, leading to a crimson solution. In a nitrogen-filled glovebox, a separate oven-dried 4 mL vial was charged with the α-hydroxy amide (0.80 mmol, 1.6 equiv.), NHC (316.5 mg, 0.80 mmol, 1.6 equiv.), and a stir bar. Methyl *tert*-butyl ether (2.5 mL) was added, and the mixture was stirred at room temperature for 5 min. Next, 4-methoxypyridine (81.2 μL, 0.80 mmol, 1.6 equiv.) was added dropwise, and the resulting solution was stirred at room temperature for another 30 min (a white solid precipitated during this time). The suspension was filtered to furnish a homogeneous solution. In a nitrogen-filled glovebox, an oven-dried 20 mL vial was charged with the aryl bromide (0.50 mmol, 1.0 equiv.), quinuclidine (67 mg, 0.60 mmol, 1.2 equiv.), phthalimide (14.7 mg, 0.10 mmol, 20.0 mol%), and a stir bar. The catalyst solution and NHC-alcohol adduct solution were transferred via syringe to the 20 mL reaction vial. The vial was transferred out of the glovebox and placed in an EtOH cooling bath at 0 °C for 5 min. Then the reaction was irradiated with blue LEDs (455 nm, 30 W) and was stirred at 0 °C for 36 h. The reaction mixture was passed through a plug of silica gel, and the vial, the cap, and the silica gel were rinsed with EtOAc. The filtrate was concentrated, and the residue was purified by flash chromatography on silica gel.

3 Results and discussion

3.1 Reaction optimization

We initially investigated the coupling reaction between lactic acid and aryl bromide. However, the presence of the hydroxy group in the carboxylic acid likely impeded the reaction, and as a result, no observable product was obtained. We then proceeded to explore the coupling reaction of its derivatives. By directly mixing a primary alkyl amine with lactic acid in the absence of a solvent, the target α-hydroxy amide was successfully obtained in good yield and subsequently evaluated in the cross-coupling reaction (Table 1).

After an extensive evaluation of all reaction parameters, we established that $NiBr_2$·DME, chiral bis(imidazoline) ligand (*S*)-**L1**, and phthalimide can accomplish the desired enantioconvergent deoxygenative reductive cross-coupling in good yield and ee (83% yield, 93% ee; entry 1). Notably, the desired coupling product acts as a potent inhibitor of fatty acid amide hydrolase (FAAH) [90]. In the absence of $NiBr_2$·DME, (*S*)-**L1**, photocatalyst, quinuclidine, or light, essentially no or only a small amount of product is observed

Table 1 Enantioconvergent deoxygenative reductive cross-coupling of a lactic acid derivative and an aryl bromide

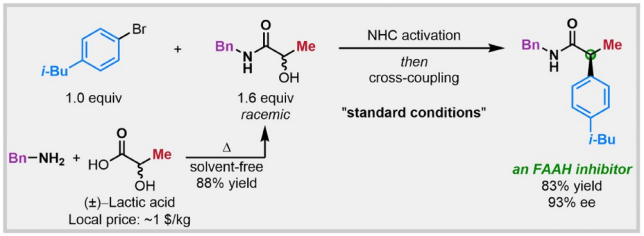

entry	variation from the "**standard conditions**"	yield (%)[a]	ee (%)[b]
1	None	83	93
2	No Ni, photocatalyst, quinuclidine, or light	0	–
3	No (*S*)-**L1**	11	0
4	No phthalimide	67	73
5	**L2**, instead of (*S*)-**L1**	81	89
6	**L3**, instead of (*S*)-**L1**	13	46
7	**L4**, instead of (*S*)-**L1**	37	-33
8	**L5**, instead of (*S*)-**L1**	0	–
9	**L6**, instead of (*S*)-**L1**	0	–
10	1.0 mL air added (4 mL vial)	75	93
11	0.1 equiv H_2O added	33	93
12	S^1 or S^3, instead of α-hydroxy amide	0	–
13	S^2, instead of α-hydroxy amide	31	22

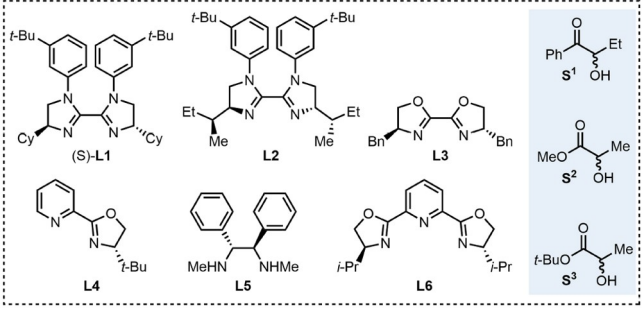

Standard reaction conditions: 1.6 equiv. 4-methoxypyridine, 1.6 equiv. NHC, MTBE, r.t., and 30 min; then 10 mol% $NiBr_2$·DME, 12 mol% (*S*)-**L1**, 20 mol% phthalimide, 1.5 mol% ($Ir[dF(CF_3)ppy]_2(dtbpy)$)PF_6, 1.2 equiv. quinuclidine, MTBE/$PhCF_3$ (1/1, 0.1 M), 455 nm blue LEDs (30 W), 0 °C, and 36 h. a) Isolated yield. b) Determined through HPLC analysis.

(racemic; entries 2 and 3). The addition of phthalimide is crucial in the deoxygenative coupling process. The absence of this additive results in a product with much lower efficiency and selectivity (entry 4). Several other chiral ligands are less effective than (*S*)-**L1** (entries 5–9). It is noteworthy that the reaction proceeds smoothly in the presence of a small amount of air (entry 10); however, the introduction of water hinders the coupling reaction (entry 11). Under these conditions, the corresponding ketone and esters are not suitable coupling partners (entries 12 and 13).

3.2 Substrate scope and applications

With the optimized reaction conditions in hand, we aimed to examine the generality of substrate scope for both coupling partners. A diverse array of lactic acid derivatives can act as useful coupling partners in this straightforward photoinduced, nickel-catalyzed enantioconvergent C–C cross-coupling reaction (Figure 2a). For example, substrates bearing various alkyl groups on the nitrogen, differing in size or containing functional groups such as ether, Boc-protected amine, and heteroaryl, have been shown to be effective in producing α-aryl amides in good yield and enantioselectivity (products **1**–**10**). In the case of an α-hydroxy amide containing a stereocenter, the stereochemistry of the chiral catalyst, rather than that of the chiral alcohol, determines the stereochemistry of the coupling product (products **11** and **12**). Furthermore, α-hydroxy-*N*-aryl-propanamides prove to be appropriate (products **13**–**16**). Impressively, not only derivatives of lactic acid but also compounds derived from other α-hydroxy carboxylic acids with varying alkyl chains can deliver the corresponding coupling products with good results (Figure 2b, products **17**–**21**).

The scope with respect to the aryl bromides is also fairly broad (Figure 2c). A variety of functional groups can be present, including fluoride, ketone, trifluoromethyl, nitrile, Bpin, tertiary alkyl alcohol, and ester; heteroaryls such as quinoline, thiophene, and dibenzothiophene are also well accommodated (products **22**–**41**). In the case of aryl bromides that bear multiple stereocenters, the stereochemistry of the chiral catalyst, rather than that of the aryl bromides, controls the stereochemistry of the coupling products (products **38**–**41**). Furthermore, the same approach can be applied to photoinduced, nickel-catalyzed enantioconvergent deoxygenative alkenylations involving trisubstituted alkenyl bromides (Figure 2d, products **42** and **43**). Through a straightforward hydrogenation process, the corresponding alkylated product is obtained (product **44**). Thus, this method offers a general strategy for synthesizing arylated, alkenylated, and alkylated coupling products. The absolute configuration of products was unambiguously determined through X-ray diffraction analysis of compound **22**.

Starting with lactic acid or lactamide, we applied our catalytic asymmetric synthesis of α-aryl amides to create various bioactive molecules and intermediates for their synthesis, including inhibitors of CXCL1 (C–X–C motif chemokine ligand 1) [91], CXCL8 [92], FAAH, and agents that inhibit neutrophil chemotaxis (Figure 2e, products **45**–**54**) [93]. It is noteworthy to point out that the primary amide (lactamide) is well tolerated in the reaction, although the enantiomeric excess is slightly lower than those observed with secondary amides (products **45**, **53**, and **54**). In the gram-scale synthesis (1.75 g of product), the coupling to generate product **49** proceeds in almost identical yield and ee as for a reaction conducted on a 0.50 mmol scale.

To further demonstrate the synthetic utility of this method, we have converted the coupling products into other valuable enantioenriched compounds (Figure 3). Specifically, α-aryl-*N*-alkyl-propanamides can be directly transformed into primary amide (with higher ee compared to that obtained from lactamide, Figure 2e), (*S*)-Ibuprofen, ester, and secondary amine, all with good yields and without racemization (products **45** and **55**–**57**).

3.3 Mechanistic experiments

Our hypothesis is that this reaction involves the potential intermediacy of an alkyl radical and that the phthalimide substituted nickel complex is the catalytic intermediate, based on previous studies and our observations of the crucial role played by phthalimide in the coupling reaction (Figure 4a). In order to understand the underlying mechanism, a series of mechanistic studies were conducted.

Cyclic voltammetry (CV) experiments were performed initially to elucidate the photoredox catalytic cycle. The NHC-alcohol adduct **N** was synthesized, and its potential, as well as that of quinuclidine (**Q**), were measured (half-wave potential $E_{1/2}$ ($\mathbf{N}^{+\cdot}$/**N**) = +0.93 V *vs*. saturated calomel electrode (SCE) in MeCN; $E_{1/2}$ ($\mathbf{Q}^{+\cdot}$/**Q**) = +1.07 V *vs*. SCE in MeCN) (for details, see Section VI of the Supporting Information). The potential of the photocatalyst (**PC**) is known (for reductive quenching: $E_{1/2}$ (**PC***/$\mathbf{PC}^{-}$) = +1.21 V *vs*. SCE in MeCN) [94]. The data presented suggests two potential pathways: (1) the excited photocatalyst directly oxidizes **N**, which is then subjected to deprotonation by quinuclidine followed by β-scission, leading to the formation of radical species (Figure 4a, path a), or (2) the excited photocatalyst initially oxidizes quinuclidine, which then abstracts hydrogen atom from **N** and undergoes β-scission to produce the radical species (Figure 4a, path b). The existence of both pathways is further supported by Stern-Volmer studies (Figure 4b). These studies show that the luminescence of the excited state of **PC** can be quenched by both **N** and quinuclidine, with **N** being a more effective quencher. This suggests that path a is the predominant pathway.

To explore the potential intermediacy of an alkyl radical,

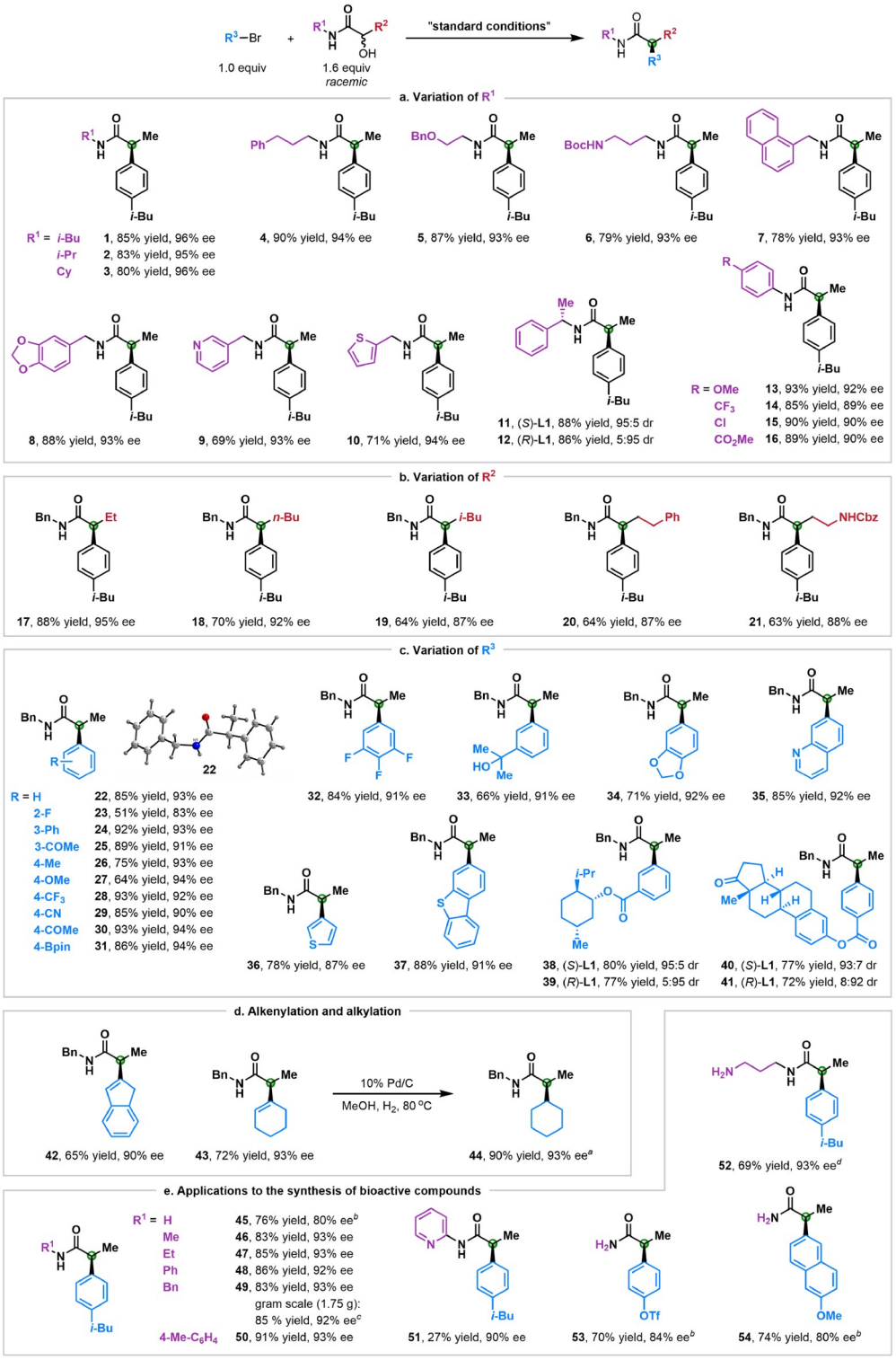

Figure 2 (Color online) Scope of the enantioconvergent deoxygenative reductive cross-coupling. All couplings were conducted on a 0.50 mmol scale (unless otherwise noted), and all yields are of purified products. (a) Variations of substituents on the nitrogen. (b) Variations of substituents at the α-position of amides. (c) Variations of aryl bromides. (d) Alkenylations and alkylation. (e) Applications to the synthesis of bioactive compounds. a) The reported yield is for the hydrogenation step. b) The compound was prepared from lactamide. c) The reaction was conducted for 48 h rather than 36 h. d) The compound was obtained through the deprotection of compound **6**, and the reported yield is the overall yield of both the coupling and deprotection reactions.

we conducted a TEMPO-trapping experiment, which formed the TEMPO-adduct **T** in 42% yield (Figure 4c). This outcome is consistent with the generation of an organic radical from the α-hydroxy amide. Our studies on coupling reactions

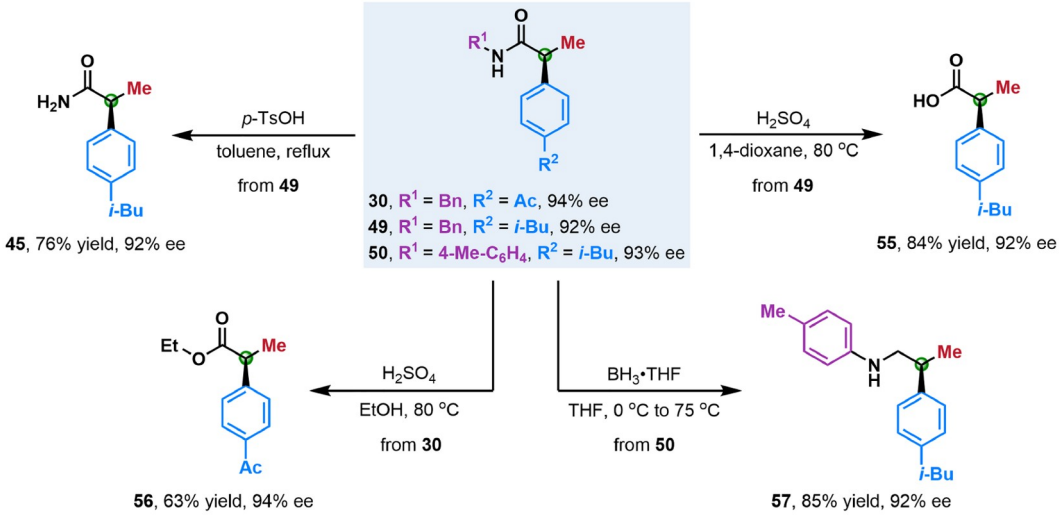

Figure 3 (Color online) Transformations into other valuable enantioenriched compounds.

involving enantiomerically enriched alkyl alcohols have also provided valuable insights. Under the standard conditions, the racemic α-hydroxy amide **S** and the two enantiomers of **S** react at similar rates in the presence of (*S*)-**L1** and the stereochemistry of the product remains unaffected by the original stereochemistry of **S** (Figure 4d, entries 1–3). These findings indicate that the coupling reaction operates as an enantioconvergent process. Furthermore, the absence of racemization of **S** during the photoinduced C–C coupling suggests that the C–O cleavage is an irreversible step.

Regarding the nickel catalytic cycle, we synthesized two key nickel intermediates, Ni-aryl bromide complex $\mathbf{Ni}^1$ and nickel-aryl phthalimide complex $\mathbf{Ni}^2$, to investigate the potential involvement of Ni(II) complexes (Figure 4e). The stoichiometric coupling of $\mathbf{Ni}^1$ with **S**, in the absence of phthalimide, affords arylation product **30** in 15% yield and 71% ee, along with the formation of homocoupling product **H** in 23% yield (Figure 4f.1, entry 1). In contrast, using $\mathbf{Ni}^2$ as an alternative yields **30** in 30% yield and 96% ee, while also generating **H** in 30% yield (Figure 4f.1, entry 2). The ee obtained with $\mathbf{Ni}^2$ is comparable to that observed under catalytic conditions (94% ee; Figure 2c, product **30**), indicating the catalytic relevance of $\mathbf{Ni}^2$ in the nickel catalytic cycle [95]. The homocoupling reaction exhibits second-order dependence on $\mathbf{Ni}^2$, which accounts for the substantial formation of **H** in the stoichiometric coupling reaction (for details, see section VI of the Supporting Information). We further examined the use of 10 mol% of either $\mathbf{Ni}^1$ or $\mathbf{Ni}^2$ as a catalyst in the cross-coupling reaction of **S**, which corroborates the previous finding. When $\mathbf{Ni}^1$ is used as the catalyst, it results in a reduced yield and enantiomeric excess (67% yield, 67% ee; Figure 4f.2, entry 1). However, adding 20 mol% of phthalimide significantly improves the outcome (94% yield, 93% ee; Figure 4f.2, entry 2). On the other hand, the employment of $\mathbf{Ni}^2$ produces the desired compound in excellent yield and enantioselectivity (96% yield, 98% ee; Figure 4f.2, entry 3). The higher ee observed with $\mathbf{Ni}^2$ as the catalyst (compared to that obtained under standard conditions) prompted us to investigate if this is a common phenomenon. To our delight, nearly all the reactions we tested provide better yield and ee when using $\mathbf{Ni}^2$ instead of the catalyst derived from $NiBr_2$·DME, (*S*)-**L1**, and phthalimide (Figure 5, products **26**–**28**, **30**, **58**, and **59**).

To further prove the role of phthalimide and the turnover-limiting step of the reaction, we carried out kinetic studies for each reaction catalyzed by $\mathbf{Ni}^1$ or $\mathbf{Ni}^2$ (for details, see section VI of the Supporting Information). In the reaction catalyzed by $\mathbf{Ni}^1$ without phthalimide, $\mathbf{Ni}^1$ is first-order dependent, whereas both alkyl alcohol and aryl bromide are zero-order dependent. However, in the reaction catalyzed by $\mathbf{Ni}^2$, both $\mathbf{Ni}^2$ and aryl bromide exhibit first-order dependence, while alkyl alcohol is zero-order dependent [96]. These findings suggest that the introduction of phthalimide may alter the turnover-limiting step, potentially shifting it to the oxidative addition of aryl bromide.

Finally, we prepared the nickel di-phthalimide complex (Ni(**L1**)$Phth_2$) and measured its potential ($E_{1/2}$ (Ni(II)/Ni(I)) = −0.82 V *vs*. SCE in MeCN; Ni(I)/Ni(0)) = −1.29 V *vs*. SCE in MeCN) (for details, see section VI of the Supporting Information). The potential of **PC** is known (for reductive quenching: $E_{1/2}$ ($\mathbf{PC}^*/\mathbf{PC}^-$) = +1.21 V *vs*. SCE in MeCN; $E_{1/2}$ ($\mathbf{PC}/\mathbf{PC}^-$) = −1.37 V *vs*. SCE in MeCN; for oxidative quenching: $E_{1/2}$ ($\mathbf{PC}^+/\mathbf{PC}^*$) = −0.89 V *vs*. SCE in MeCN; $E_{1/2}$ ($\mathbf{PC}^+/\mathbf{PC}$) = +1.69 V *vs*. SCE in MeCN) [97]. While both $\mathbf{PC}^*$ and $\mathbf{PC}^+$ can oxidize **N** ($E_{1/2}$ ($\mathbf{N}^{+\cdot}/\mathbf{N}$) = +0.93 V *vs*. SCE in MeCN), only $\mathbf{PC}^-$ can reduce Ni(**L1**)Phth to Ni(0), whereas $\mathbf{PC}^*$ can hardly do so (−0.89 V *vs*. −1.29 V). Therefore, it can be concluded that the photoinduced

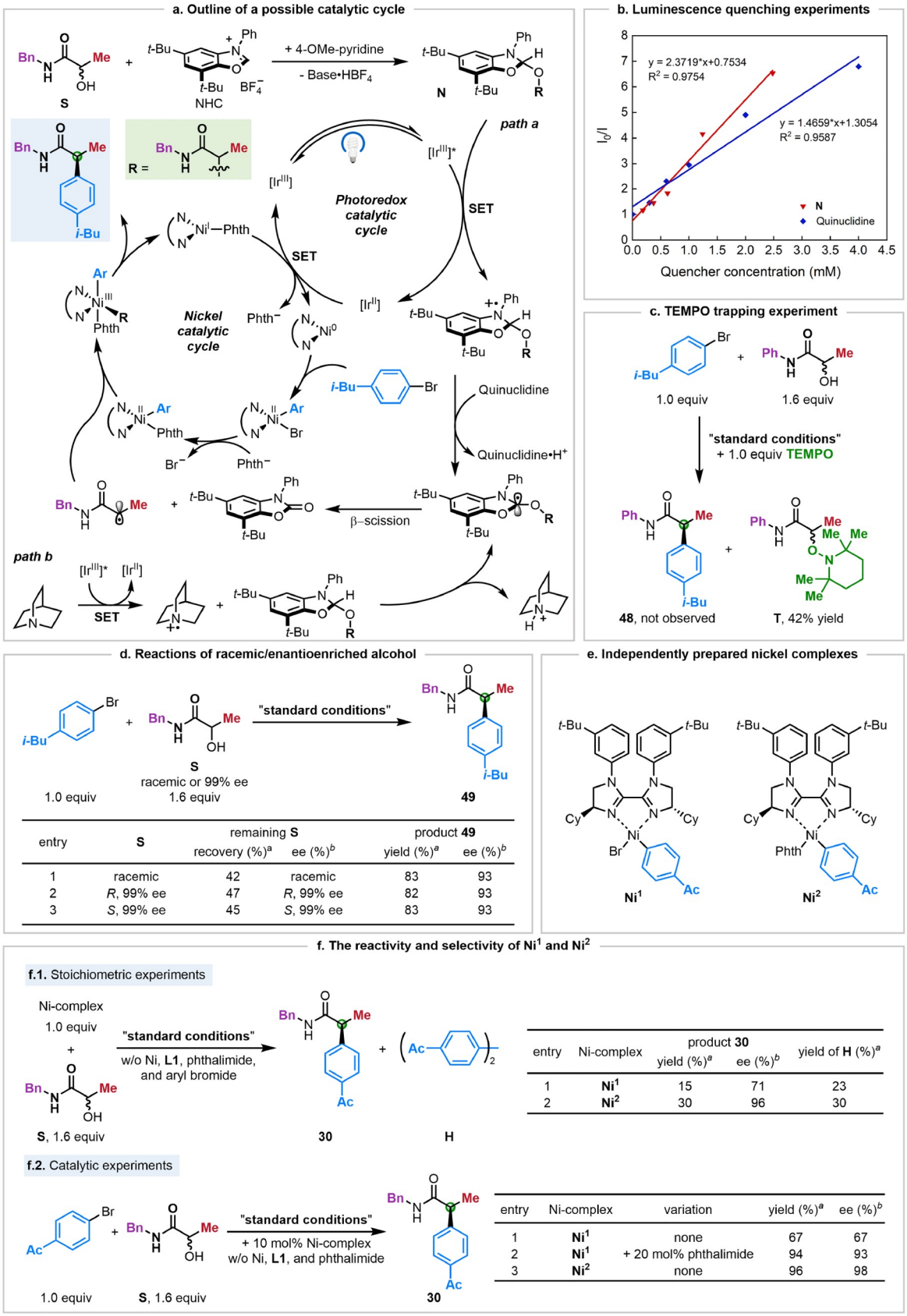

entry	S	remaining S recovery (%)[a]	remaining S ee (%)[b]	product 49 yield (%)[a]	product 49 ee (%)[b]
1	racemic	42	racemic	83	93
2	*R*, 99% ee	47	*R*, 99% ee	82	93
3	*S*, 99% ee	45	*S*, 99% ee	83	93

entry	Ni-complex	product 30 yield (%)[a]	product 30 ee (%)[b]	yield of H (%)[a]
1	**Ni¹**	15	71	23
2	**Ni²**	30	96	30

entry	Ni-complex	variation	yield (%)[a]	ee (%)[b]
1	**Ni¹**	none	67	67
2	**Ni¹**	+ 20 mol% phthalimide	94	93
3	**Ni²**	none	96	98

Figure 4 (Color online) Mechanism. (a) Outline of a possible catalytic cycle. (b) Luminescence quenching experiments. (c) Radical trapping experiment. (d) Cross-coupling reactions starting from racemic or enantioenriched alkyl alcohols. (e) Independently prepared nickel complexes. (f) The reactivity and selectivity of the independently prepared nickel complexes. a) Isolated yield. b) Determined through HPLC analysis.

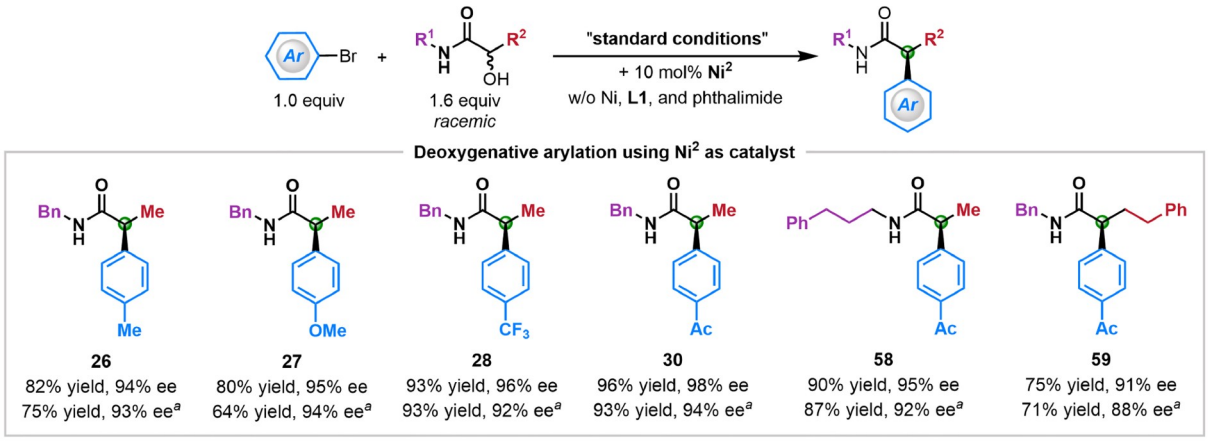

Figure 5 (Color online) Catalytic asymmetric synthesis of α-aryl amides by using $\mathbf{Ni^2}$ as the catalyst. All couplings were conducted on a 0.50 mmol scale (unless otherwise noted), and all yields are of purified products. a) Results obtained under standard conditions.

electron transfer proceeds through a reductive quenching mechanism.

3.4 DFT calculations

Inspired by the findings in our mechanistic studies and the mechanisms of similar reactions proposed in the literature [98,99], we performed DFT calculations of the reaction profile with (*S*)-**L1** ligand (Table 1, "standard conditions"). The electronic energies with solvation energy corrections were calculated by using PW6B95-D3/BS2/SMD//B3LYP/BS1 level of theory with Gaussian 16 program (BS1: 6-31G(d) for C, H, O, N, Br and def2-SVP for Ni; BS2: 6-311G(d,p) for C, H, O, N, Br and def2-TZVP for Ni) [100–109]. The thermal corrections for Gibbs free energies were calculated at 273 K by using the Shermo program [110]. As shown in Figure 6, the initial state (**IS**) of Ni(0) coordinated with (*S*)-**L1** and aryl bromide undergoes an oxidative addition with 3.89 kcal/mol energy barrier (**TS1**) to form a square-planer Ni(II) complex **IM1** in singlet spin state. This complex then undergoes isomerization to form a tetrahedral Ni(II) complex **IM2** in a triplet spin state with lower energy (Figure 4e, $\mathbf{Ni^1}$). The α-hydroxy amide **S** undergoes a single-electron transfer (SET) to form a relatively stable alkyl radical as shown by experiments (Figure 4c). The radical is then added to **IM2** to form Ni(III) complex **IM3** through an oxidative addition process, which subsequently undergoes reductive elimination to generate **FS1** consisting of a Ni(I) complex and the product. The addition of alkyl radical is the key enantio-determining step. The rate constant can be expressed by transition state theory as $k = Ae^{-\Delta G/RT}$, so the ee can be calculated using the equation $ee = (e^{-\Delta\Delta G/RT} - 1)/(e^{-\Delta\Delta G/RT} + 1)$, in which $\Delta\Delta G$ represents the Gibbs free energy difference between the two transition states in the enantio-determining step. In the reaction without phthalimide, ΔG(**TS2-S**) − ΔG(**TS2-R**) = −0.94 kcal/mol, rendering 70% ee that agrees with experimental observations (73% ee; Table 1, entry 4). Throughout the whole reaction profile, the highest energy barriers in the pathways leading to (*S*)-product and (*R*)-product are 9.53 kcal/mol (**TS2-S**) and 10.47 kcal/mol (**TS2-R**) respectively, meaning the oxidative addition of alkyl radical to **IM2** is not only the enantio-determining step but also the rate-determining step, also in agreement with experimental findings.

In the reaction with phthalimide, the phthalimide ion replaces the bromide ion in a rapid ligand exchange with 3.10 kcal/mol energy barrier (**TS4**) to form a Ni(II) complex **IM4** that has been identified as a key catalytic intermediate (Figure 4e, $\mathbf{Ni^2}$). The subsequent reaction pathways would be quite similar to those under conditions without phthalimide: (1) the alkyl radical is added to **IM4** to form Ni(III) complex **IM5** through an oxidative addition process, which is also an enantio-determining step, and (2) **IM5** undergoes reductive elimination to generate **FS2**, consisting of a Ni(I) complex and the product. Compared to the reaction without phthalimide, the energy difference between the two transition states in the enantio-determining step is larger, ΔG(**TS5-S**) − ΔG(**TS5-R**) = −1.28 kcal/mol, rendering 83% ee that is slightly lower than the experimental value (93% ee; Table 1, entry 1). It is noteworthy that the introduction of phthalimide decreases the energy barrier of radical addition and the following reductive elimination, thus changing the rate-determining step. In the reaction pathway that generates (*S*)-product, the energy barriers of **TS4**, **TS5-S**, and **TS6-S** are 3.10, 3.15, and 0.28 kcal/mol respectively, which are all smaller than the energy barrier of **TS1** (3.89 kcal/mol). This makes the step involving the oxidation addition of aryl bromide the rate-determining step, which is consistent with our experimental kinetic studies. In the reaction pathway that generates (*R*)-product, the energy barriers of **TS5-R** and **TS6-R** are also decreased compared to **TS2-R** and **TS3-R**, but still higher than those of **TS5-S** and **TS6-S**, so that the

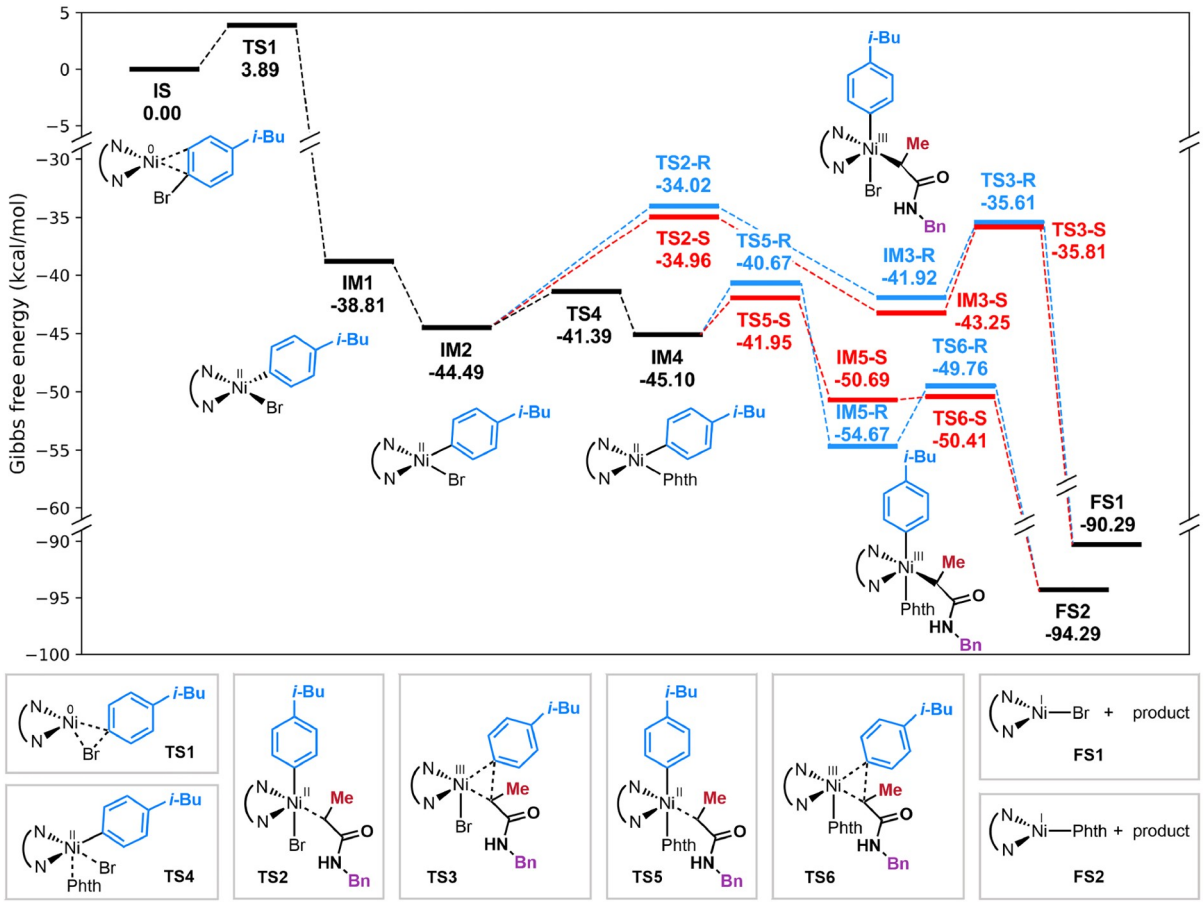

Figure 6 (Color online) Reaction energy profile. Structures of initial state (**IS**) and intermediate states (**IM**) are drawn in the energy profile, and structures of transition states (**TS**) and final states (**FS**) are drawn below. Blue lines represent the reaction pathways leading to (*R*)-product, and red lines represent the reaction pathways leading to (*S*)-product. **IM2**, **TS4**, and **IM4** are in triplet spin states, all the other molecules are in their lowest possible spin states (singlet or doublet).

reaction pathway leading to (*S*)-product is dominating. The introduction of phthalimide reduces the overall energy barriers from 9.53 to 3.89 kcal/mol for (*S*)-product and from 10.47 to 4.91 kcal/mol for (*R*)-product, accelerating the reactions so that more desired products are generated, and relatively fewer side products are generated, thereby increasing the yield as well.

Although the calculations slightly underestimate the ee, they demonstrate that the energy barrier change of the enantio-determining step is the key to the increased enantioselectivity when phthalimide is added. Figure 7 shows the key transition states in ball-and-stick models and Newman projections with C in the front and Ni in the back. For **TS2-R** and **TS2-S**, the H atom on the amide group (–CONH) forms weak bonding with the electronegative atom Br, leaving the methyl group in gauche (60° tilt) position with respect to Br in **TS2-R** but in anti (180° tilt) position with respect to Br in **TS2-S**. Although the aryl group is closer to the methyl group in **TS2-S** than in **TS2-R**, it reduces steric strain by rotating the aryl group around Ni to some extent. In contrast, the Br is more rigid due to bonding with the amide group, and the repulsion between Br and the methyl group is why **TS2-S** has less steric strain than **TS2-R**. Similarly, for **TS5-S** and **TS5-R**, the H atom on the amide group forms hydrogen bonding with the O atom on phthalimide, so that the methyl group collides with phthalimide in gauche (60° tilt) position in **TS5-R** but avoids the collision in **TS5-S**. The aryl group also rotates around Ni to reduce steric strain with the methyl group in **TS5-S**. Because phthalimide is rigid due to hydrogen bonding and is a larger group than Br, **TS5-R** suffers from more steric strain than **TS2-R**, causing a larger energy difference between **TS5-S** and **TS5-R** than that between **TS2-S** and **TS2-R**.

3.5 Proposed catalytic cycle

Based on the above observations and prior studies, a possible catalytic cycle for the model reaction is proposed in Figure 4a. The reaction initiates with the condensation of alkyl alcohol **S** and NHC to produce an NHC-alcohol adduct **N**. Concurrently, irradiation of the iridium photocatalyst [Ir^{III}] with blue light-emitting diodes (LEDs) generates a

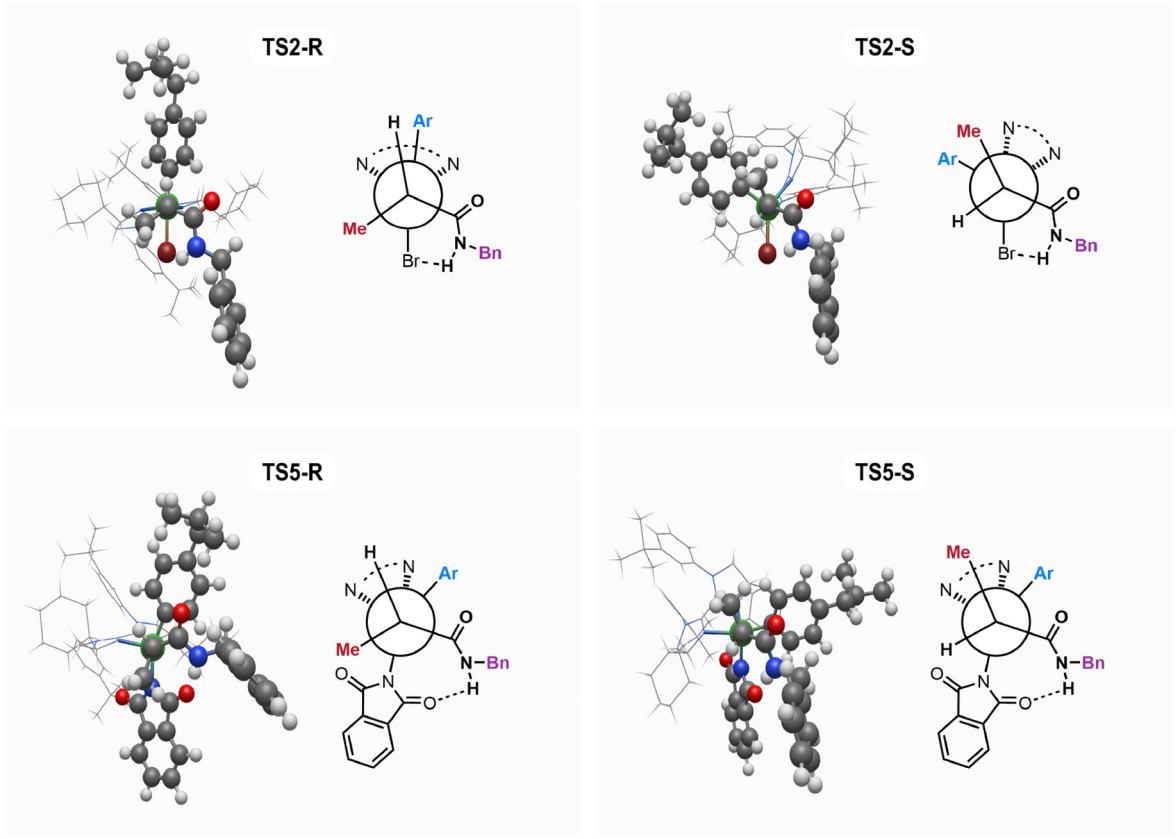

Figure 7 (Color online) Structures of transition states. Ligand is shown in wireframe display format. Colors for the other atoms, grey: C, white: H, red: O, blue: N, maroon: Br, green: Ni.

long-lived excited-state complex [Ir^{III}]* (2.3 μs). This highly oxidizing charge transfer species facilitates an SET through either path a or path b, leading to the formation of reduced [Ir^{II}] and a crucial alkyl radical. In the nickel catalytic cycle, the oxidative addition of Ni(0) to aryl bromide results in the formation of a Ni-aryl bromide species (the rate-determining step), which then undergoes a rapid ligand substitution to form a Ni-aryl phthalimide complex. The alkyl radical is trapped, leading to the generation of a key Ni(III) species (the enantio-determining step), which then undergoes reductive elimination to produce the coupling product and Ni(**L1**)Phth. Finally, Ni(I) is reduced by [Ir^{II}] to regenerate Ni(0).

4 Conclusions

By exploiting photoinduced nickel catalysis, we have accomplished enantioconvergent deoxygenative reductive cross-coupling reactions of lactic acid derivatives, facilitating a convergent approach to the asymmetric synthesis of α-aryl amides, wherein both C–O bond cleavage and C–C bond formation are achieved in a one-pot process. The method employs two classes of ligands to assemble the active catalyst *in situ*: chiral bis(imidazoline) ligand (*S*)-**L1** and phthalimide, which coordinate with Ni(II) to enhance both the efficiency and selectivity of the C–C bond formation. This catalyst demonstrates versatility, being capable of catalyzing not only asymmetric arylation but also alkenylation, thus enabling the generation of arylated, alkenylated, and alkylated coupling products. The synthetic utility has been validated through the rapid synthesis of various bioactive molecules. Additionally, a comprehensive mechanistic study has clarified the role of phthalimide and the reaction pathway.

Acknowledgements This work was supported by the National Natural Science Foundation of China (22201216 to Ze-Peng Yang), the National Key Research & Development Program of China (2023YFA1508600 to Ze-Peng Yang), and the Fundamental Research Funds for the Central Universities (22120240079 to Ze-Peng Yang, and 22120230504 to Kaining Duanmu).

Conflict of interest The authors declare no conflict of interest.

Supporting information The supporting information is available online at http://chem.scichina.com and http://link.springer.com/journal/11426. The supporting materials are published as submitted, without typesetting or editing. The responsibility for scientific accuracy and content remains entirely with the authors.

1 Castillo Martinez FA, Balciunas EM, Salgado JM, Domínguez González JM, Converti A, Oliveira RPS. *Trends Food Sci Tech*, 2013, 30: 70–83
2 https://www.researchandmarkets.com/reports/4751812/global-lactic-acid-market-size-share-and-trends, accessed on 2024-10-05
3 Datta R, Henry M. *J Chem Tech Biotech*, 2006, 81: 1119–1129
4 Dusselier M, Van Wouwe P, Dewaele A, Makshina E, Sels BF. *Energy Environ Sci*, 2013, 6: 1415–1442
5 Song S, Qu J, Han P, Hülsey MJ, Zhang G, Wang Y, Wang S, Chen D, Lu J, Yan N. *Nat Commun*, 2020, 11: 4899
6 Peng TY, Xu ZY, Zhang FL, Li B, Xu WP, Fu Y, Wang YF. *Angew Chem Int Ed*, 2022, 61: e202201329
7 Han YW, Ye L, Gong TJ, Fu Y. *Angew Chem Int Ed*, 2023, 62: e202306305
8 Cheng L, Lin Q, Chen Y, Gong H. *Synthesis*, 2022, 54: 4426–4446
9 Pang X, Su PF, Shu XZ. *Acc Chem Res*, 2022, 55: 2491–2509
10 Huang CY, Li J, Li CJ. *Chem Sci*, 2022, 13: 5465–5504
11 Anwar K, Merkens K, Aguilar Troyano FJ, Gómez-Suárez A. *Eur J Org Chem*, 2022, 2022: e202200330
12 Pang X, Shu XZ. *Chin J Chem*, 2023, 41: 1637–1652
13 Mandal T, Mallick S, Islam M, De Sarkar S. *ACS Catal*, 2024, 14: 13451–13496
14 Blanksby SJ, Ellison GB. *Acc Chem Res*, 2003, 36: 255–263
15 Diéguez HR, López A, Domingo V, Arteaga JF, Dobado JA, Herrador MM, Quílez del Moral JF, Barrero AF. *J Am Chem Soc*, 2010, 132: 254–259
16 Suga T, Shimazu S, Ukaji Y. *Org Lett*, 2018, 20: 5389–5392
17 Stache EE, Ertel AB, Rovis T, Doyle AG. *ACS Catal*, 2018, 8: 11134–11139
18 Suga T, Ukaji Y. *Org Lett*, 2018, 20: 7846–7850
19 Suga T, Takahashi Y, Ukaji Y. *Adv Synth Catal*, 2020, 362: 5622–5626
20 Xie H, Guo J, Wang YQ, Wang K, Guo P, Su PF, Wang X, Shu XZ. *J Am Chem Soc*, 2020, 142: 16787–16794
21 Sumiyama K, Toriumi N, Iwasawa N. *Eur J Org Chem*, 2021, 2021 (17): 2474–2478
22 Xie H, Wang S, Wang Y, Guo P, Shu XZ. *ACS Catal*, 2022, 12: 1018–1023
23 Suga T, Takahashi Y, Miki C, Ukaji Y. *Angew Chem Int Ed*, 2022, 61: e202112533
24 Suga T, Takada R, Shimazu S, Sakata M, Ukaji Y. *J Org Chem*, 2022, 87: 7487–7493
25 Lin Q, Tong W, Shu XZ, Chen Y. *Org Lett*, 2022, 24: 8459–8464
26 Li WD, Wu Y, Li SJ, Jiang YQ, Li YL, Lan Y, Xia JB. *J Am Chem Soc*, 2022, 144: 8551–8559
27 Nawrat CC, Jamison CR, Slutskyy Y, MacMillan DWC, Overman LE. *J Am Chem Soc*, 2015, 137: 11270–11273
28 Ackerman LKG, Anka-Lufford LL, Naodovic M, Weix DJ. *Chem Sci*, 2015, 6: 1115–1119
29 Konev MO, Hanna LE, Jarvo ER. *Angew Chem Int Ed*, 2016, 55: 6730–6733
30 Zhang X, MacMillan DWC. *J Am Chem Soc*, 2016, 138: 13862–13865
31 Vara BA, Patel NR, Molander GA. *ACS Catal*, 2017, 7: 3955–3959
32 Ye Y, Chen H, Sessler JL, Gong H. *J Am Chem Soc*, 2019, 141: 820–824
33 Friese FW, Studer A. *Angew Chem Int Ed*, 2019, 58: 9561–9564
34 Cai A, Yan W, Liu W. *J Am Chem Soc*, 2021, 143: 9952–9960
35 Jana SK, Bhattacharya R, Dey P, Chakraborty S, Maji B. *ACS Catal*, 2024, 14: 14172–14182
36 Majhi J, Matsuo B, Oh H, Kim S, Sharique M, Molander GA. *Angew Chem Int Ed*, 2024, 63: e202317190
37 Zheng X, Dai XJ, Yuan HQ, Ye CX, Ma J, Huang PQ. *Angew Chem Int Ed*, 2013, 52: 3494–3498
38 Guo P, Wang K, Jin WJ, Xie H, Qi L, Liu XY, Shu XZ. *J Am Chem Soc*, 2021, 143: 513–523
39 Li Z, Sun W, Wang X, Li L, Zhang Y, Li C. *J Am Chem Soc*, 2021, 143: 3536–3543
40 Lin Q, Ma G, Gong H. *ACS Catal*, 2021, 11: 14102–14109
41 Chi BK, Widness JK, Gilbert MM, Salgueiro DC, Garcia KJ, Weix DJ. *ACS Catal*, 2022, 12: 580–586
42 Cook A, St. Onge P, Newman SG. *Nat Synth*, 2023, 2: 663–669
43 Xu W, Fan C, Hu X, Xu T. *Angew Chem Int Ed*, 2024, 63: e202401575
44 Dong Z, MacMillan DWC. *Nature*, 2021, 598: 451–456
45 Wang JZ, Sakai HA, MacMillan DWC. *Angew Chem Int Ed*, 2022, 61: e202207150
46 Sakai HA, MacMillan DWC. *J Am Chem Soc*, 2022, 144: 6185–6192
47 Intermaggio NE, Millet A, Davis DL, MacMillan DWC. *J Am Chem Soc*, 2022, 144: 11961–11968
48 Carson II WP, Sarver PJ, Goudy NS, MacMillan DWC. *J Am Chem Soc*, 2023, 145: 20767–20774
49 Lyon WL, MacMillan DWC. *J Am Chem Soc*, 2023, 145: 7736–7742
50 Gould CA, Pace AL, MacMillan DWC. *J Am Chem Soc*, 2023, 145: 16330–16336
51 Bissonnette NB, Bisballe N, Tran AV, Rossi-Ashton JA, MacMillan DWC. *J Am Chem Soc*, 2024, 146: 7942–7949
52 Wang JZ, Lyon WL, MacMillan DWC. *Nature*, 2024, 628: 104–109
53 Chen R, Intermaggio NE, Xie J, Rossi-Ashton JA, Gould CA, Martin RT, Alcázar J, MacMillan DWC. *Science*, 2024, 383: 1350–1357
54 Mao E, Prieto Kullmer CN, Sakai HA, MacMillan DWC. *J Am Chem Soc*, 2024, 146: 5067–5073
55 Carson II WP, Tsymbal AV, Pipal RW, Edwards GA, Martinelli JR, Cabré A, MacMillan DWC. *J Am Chem Soc*, 2024, 146: 15681–15687
56 Cai Q, McWhinnie IM, Dow NW, Chan AY, MacMillan DWC. *J Am Chem Soc*, 2024, 146: 12300–12309
57 Döben N, Reimler J, Studer A. *Adv Synth Catal*, 2022, 364: 3348–3353
58 Sanosa N, Ambrosi D, Ruiz-Campos P, Sampedro D, Funes-Ardoiz I. *Chem Eur J*, 2023, 29: e202301406
59 Bai T, Li H. *J Org Chem*, 2024, 89: 5363–5370
60 Li Z, Wang L, Zeng T, Huang Z, Song S, Qi X, Zhu J. *ACS Catal*, 2024, 14: 9496–9504
61 Song S, Li Z, Wang L, Zeng T, Hu Q, Zhu J. *Org Lett*, 2024, 26: 264–268
62 Wang L, Li Z, Zhou Y, Zhu J. *Org Lett*, 2024, 26: 2297–2302
63 Liu DP, Zhang XS, Liu S, Hu XG. *Nat Commun*, 2024, 15: 3401
64 Xiong W, Kang T, Li F, Liao H, Yan Y, Dong J, Li G, Xue D. *ACS Catal*, 2024, 14: 14089–14097
65 Wang Q, Tian Y, Han D, Xiao W, Ma M, Zhao B. *Org Chem Front*, 2024, 11: 3471–3477
66 Zeng H, Yin R, Zhao Y, Ma JA, Wu J. *Nat Chem*, 2024, 16: 1822–1830
67 Geist E, Kirschning A, Schmidt T. *Nat Prod Rep*, 2014, 31: 441–448
68 Cherney AH, Kadunce NT, Reisman SE. *Chem Rev*, 2015, 115: 9587–9652
69 Iwasaki T, Kambe N. *Top Curr Chem (Z)*, 2016, 374: 66
70 Fu GC. *ACS Cent Sci*, 2017, 3: 692–700
71 Choi J, Fu GC. *Science*, 2017, 356: eaaf7230
72 Ke Y, Li W, Liu W, Kong W. *Sci China Chem*, 2023, 66: 2951–2976
73 DeLano TJ, Reisman SE. *ACS Catal*, 2019, 9: 6751–6754
74 Guan H, Zhang Q, Walsh PJ, Mao J. *Angew Chem Int Ed*, 2020, 59: 5172–5177
75 Min Y, Sheng J, Yu JL, Ni SX, Ma G, Gong H, Wang XS. *Angew Chem Int Ed*, 2021, 60: 9947–9952
76 Lau SH, Borden MA, Steiman TJ, Wang LS, Parasram M, Doyle AG. *J Am Chem Soc*, 2021, 143: 15873–15881
77 Sun D, Tao X, Ma G, Wang J, Chen Y. *Chem Sci*, 2022, 13: 8365–8370
78 He Y, Ma J, Song H, Zhang Y, Liang Y, Wang Y, Zhu S. *Nat Commun*, 2022, 13: 2471
79 Zhao WT, Zhang JX, Chen BH, Shu W. *Nat Commun*, 2023, 14: 2938

80 Peng JH, Zheng YQ, Bai LG, Liu WB. *Sci China Chem*, 2023, 66: 3148–3153
81 Zhou J, Wang D, Xu W, Hu Z, Xu T. *J Am Chem Soc*, 2023, 145: 2081–2087
82 Li X, Yuan M, Chen F, Huang Z, Qing FL, Gutierrez O, Chu L. *Chem*, 2023, 9: 154–169
83 Gao Y, Zhang B, He J, Baran PS. *J Am Chem Soc*, 2023, 145: 11518–11523
84 Lin D, Chen Y, Dong Z, Pei P, Ji H, Tai L, Chen LA. *CCS Chem*, 2023, 5: 1386–1397
85 Li J, Cheng B, Shu X, Xu Z, Li C, Huo H. *Nat Catal*, 2024, 7: 889–899
86 Zhang LL, Gao YZ, Cai SH, Yu H, Shen SJ, Ping Q, Yang ZP. *Nat Commun*, 2024, 15: 2733
87 Do HQ, Chandrashekar ERR, Fu GC. *J Am Chem Soc*, 2013, 135: 16288–16291
88 Chen HW, Lu FD, Cheng Y, Jia Y, Lu LQ, Xiao WJ. *Chin J Chem*, 2020, 38: 1671–1675
89 Han GY, Su PF, Pan QQ, Liu XY, Shu XZ. *Nat Catal*, 2024, 7: 12–20
90 Deplano A, Cipriano M, Moraca F, Novellino E, Catalanotti B, Fowler CJ, Onnis V. *J Enzyme Inhib Med Chem*, 2019, 34: 562–576
91 Moriconi A, Bigogno C, Bianchini G, Caligiuri A, Resconi A, Dondio MG, D'Anniballe G, Allegretti M. *ACS Med Chem Lett*, 2011, 2: 768–773
92 Allegretti M, Bertini R, Cesta MC, Bizzarri C, Di Bitondo R, Di Cioccio V, Galliera E, Berdini V, Topai A, Zampella G, Russo V, Di Bello N, Nano G, Nicolini L, Locati M, Fantucci P, Florio S, Colotta F. *J Med Chem*, 2005, 48: 4312–4331
93 Allegretti M, Bertini R, Berdini V, Bizzarri C, Cesta MC, Di Cioccio V, Caselli G, Colotta F, Gandolfi C, Gandolfi JPB, Gandolfi GA, Gandolfi MC, Gandolfi AA. Omega Aminoalkylamides of R-2 Aryl Propionic Acids as Inhibitors of the Chemotaxis of Polymorphonucleate and Mononucleate Cells. United States Patent, US 8288368B2, 2012
94 Corrigan N, Shanmugam S, Xu J, Boyer C. *Chem Soc Rev*, 2016, 45: 6165–6212
95 Prieto Kullmer CN, Kautzky JA, Krska SW, Nowak T, Dreher SD, MacMillan DWC. *Science*, 2022, 376: 532–539
96 Our kinetic studies suggest that both the $\mathbf{Ni}^{\mathbf{I}}$ and $\mathbf{Ni}^{\mathbf{II}}$ catalyzed pathways may coexist when $\mathbf{Ni}^{\mathbf{II}}$ is used as the catalyst. The aryl bromide serves as the source of bromide, facilitating the generation of $\mathbf{Ni}^{\mathbf{I}}$ as the reaction proceeds
97 The photoinduced electron transfer process can occur in two distinct ways: (i) reductive quenching, whereby the photocatalyst accepts an electron from a reductant, or (ii) oxidative quenching, whereby the photocatalyst donates an electron to an oxidant
98 Wang H, Liu CF, Song Z, Yuan M, Ho YA, Gutierrez O, Koh MJ. *ACS Catal*, 2020, 10: 4451–4459
99 Matsui JK, Gutiérrez-Bonet Á, Rotella M, Alam R, Gutierrez O, Molander GA. *Angew Chem Int Ed*, 2018, 57: 15847–15851
100 Gaussian 16, Revision C.01, Frisch MJ, Trucks GW, Schlegel HB, Scuseria GE, Robb MA, Cheeseman JR, Scalmani G, Barone V, Petersson GA, Nakatsuji H, Li X, Caricato M, Marenich AV, Bloino J, Janesko BG, Gomperts R, Mennucci B, Hratchian HP, Ortiz JV, Izmaylov AF, Sonnenberg JL, Williams-Young D, Ding F, Lipparini F, Egidi F, Goings J, Peng B, Petrone A, Henderson T, Ranasinghe D, Zakrzewski VG, Gao J, Rega N, Zheng G, Liang W, Hada M, Ehara M, Toyota K, Fukuda R, Hasegawa J, Ishida M, Nakajima T, Honda Y, Kitao O, Nakai H, Vreven T, Throssell K, Montgomery JAJ, Peralta JE, Ogliaro F, Bearpark MJ, Heyd JJ, Brothers EN, Kudin KN, Staroverov VN, Keith TA, Kobayashi R, Normand J, Raghavachari K, Rendell AP, Burant JC, Iyengar SS, Tomasi J, Cossi M, Millam JM, Klene M, Adamo C, Cammi R, Ochterski JW, Martin RL, Morokuma K, Farkas O, Foresman JB, Fox DJ. Gaussian, Inc. Wallingford CT, 2016
101 Zhao Y, Truhlar DG. *J Phys Chem A*, 2005, 109: 5656–5667
102 Grimme S, Antony J, Ehrlich S, Krieg H. *J Chem Phys*, 2010, 132: 154104
103 Becke AD. *J Chem Phys*, 1993, 98: 5648–5652
104 Lee C, Yang W, Parr RG. *Phys Rev B*, 1988, 37: 785–789
105 Miehlich B, Savin A, Stoll H, Preuss H. *Chem Phys Lett*, 1989, 157: 200–206
106 Marenich AV, Cramer CJ, Truhlar DG. *J Phys Chem B*, 2009, 113: 6378–6396
107 Ditchfield R, Hehre WJ, Pople JA. *J Chem Phys*, 1971, 54: 724–728
108 Weigend F, Ahlrichs R. *Phys Chem Chem Phys*, 2005, 7: 3297–3305
109 Weigend F. *Phys Chem Chem Phys*, 2006, 8: 1057–1065
110 Lu T, Chen Q. *Comput Theor Chem*, 2021, 1200: 113249